Available online at www.sciencedirect.com
SCIENCE DIRECT®
International Journal of Heat and Mass Transfer 48 (2005) 211–225
International Journal of HEAT and MASS TRANSFER
www.elsevier.com/locate/ijhmt

Two-phase phase distribution in a vertical large diameter pipe

Xiuzhong Shen [a], Kaichiro Mishima [a,*], Hideo Nakamura [b]

[a] Research Reactor Institute, Kyoto University, Kumatori-cho, Sennan-gun, Osaka 590-0494, Japan
[b] Tokai Establishment, Japan Atomic Energy Research Institute, Tokai-mura, Naka-gun, Ibaraki 319-1195, Japan

Received 19 September 2003
Available online 22 October 2004

Abstract

In view of the practical importance of the application of two-phase flow in a large diameter pipe to various fields of engineering, the characteristics and phase distribution patterns of two-phase flow in a vertical large diameter pipe have been experimentally and theoretically studied for various flow conditions. The local measurements for the interfacial parameters (void fraction, Sauter mean diameter and pressure loss) in a vertical upward air–water two-phase flow in a pipe with 0.2 m in inner diameter and 24 m in height have been performed by using the optical probes and differential pressure transducers. The two-phase flow characteristics have been analyzed with experimental data, which shows that the phase distribution patterns in the vertical large diameter pipe can be divided into two basic patterns, namely, wall peak and core peak. With the application of the concept of skewness, the two-phase distribution patterns have been quantitatively distinguished by establishing a phase distribution pattern transition criterion. An empirical relation for the phase distribution transition from wall peak to core peak was fitted by using the phase distribution pattern transition criterion and the present experimental data and verified by other researchers' experimental data. This study also showed that there existed the flow plugging phenomena in the low region of the test section at high superficial gas velocity conditions in the vertical large diameter pipe.

Keywords: Gas–liquid two-phase flows; Skewness; Phase distribution patterns and transition; Flow plugging; Large diameter pipe

1. Introduction

A large diameter pipe systems with gas–liquid two-phase flow are often encountered in various fields of engineering such as nuclear power plant, chemical industry, petroleum transport pipes and so on. In order to analyze the thermal hydraulics of two-phase flow in a large diameter pipe, it is fundamentally important to understand the complex characteristics of gas–liquid two-phase flow, particularly the phase distribution mechanisms of the flow in a large diameter pipe.

Much experimental work [1–7] has been performed for phase distributions under various conditions. Nevertheless, phase distribution mechanisms have been yet least understood. One of the major difficulties in the prediction of phase distribution in gas–liquid two-phase flow is the fact that the phase distribution is strongly linked with the interfacial structures and motions. The flow in a large diameter pipe is characterized by the strong bubble induced turbulence or secondary flow. The phase distribution mechanism in a large diameter

* Corresponding author. Tel.: +81 724 51 2449; fax: +81 724 51 2637.
E-mail address: mishima@rri.kyoto-u.ac.jp (K. Mishima).

0017-9310/$ - see front matter © 2004 Elsevier Ltd. All rights reserved.
doi:10.1016/j.ijheatmasstransfer.2004.06.034

Nomenclature

A	cross-sectional area
B	central moment
D	pipe diameter
D_{SM}	Sauter mean diameter
d_{bl}	the length along the major axis for a distorted ellipsoidal bubble
F	an arbitrary parameter
j	superficial velocity
R	inner radius of a pipe
Re	Reynolds number
r	radial distance
z	axial distance

Greek symbols

α	time-averaged void fraction
γ	(Fisher) skewness
μ	viscosity
ρ	density

Subscripts

DP	differential pressure
f	liquid phase
g	gas phase
i	the ith central moment, $i = 1, 2, 3$
Probe	optical probe

Mathematical symbol

$\langle\cdot\rangle$	area-averaged quantity over cross-sectional flow area

pipe is expected to be different from that in a small round tube. This study focuses on the air-liquid two-phase flow characteristics in a large diameter pipe so as to get a better understand of the phase distribution mechanism in a large diameter pipe.

2. Experimental

2.1. Experimental rig

The present study was carried out by using the Large Scale Test Facility (LSTF) in the Japanese Atomic Energy Research Institute (JAERI). Fig. 1 shows the experimental facility layout. The purified water was used in the experimental loop and replaced everyday during the experimental period to maintain the water quality. The water supply was held in the lower reservoir tank. Water was pumped with a positive displacement, centrifugal pump, capable of providing a constant head with minimum pressure oscillation. For the adiabatic air–water flow experiment, a porous ring sinter tube with grain size of 40 μm and 2×80 holes of $\varnothing$ 0.5 mm was used as air injectors. The water, which flowed through one Venturi flow meter, was divided into four separate flows and can then be mixed with air, while the water, which flowed through the other Venturi flow meter, was divided into two separate flows and then mixed with the former mixed air–water flow before they were injected into the test section to study adiabatic air–water two-phase flow. The water temperature was kept at a constant temperature (25 °C) within the deviation of ±1 °C by a cooler installed in the lower reservoir tank. Due to the high pressure in the low part of the facility, the test section was made of stainless steel and transparent acrylic resin round pipes for its solidity and flow observation respectively. All of the pipes in the test section were 200 mm in inner diameter. The overall height of the test section was about 24 m, not including the height of the upper reservoir tank. The two-phase mixture flowed out of the test section to a separator, namely, the open upper reservoir tank. The air was discharged there and the water circulates through the loop.

2.2. Instrumentation and data acquisition system

The inlet water flow rate and pressure were measured by using Venturi flow meters (25 and 50 mm in inner diameters, respectively) and pressure gage respectively and the inlet gas flow rate and pressure were measured by using FE-H11-GAS and FE-H12-GAS orifice flow meters and pressure gage, respectively. The pressure distribution along the flow was obtained by using differential pressure transducers. Optical probes, i.e. conical- or flat-tip double-sensor (c2s or f2s) or flat-tip four-sensor optical probes have been arranged at 3 axial locations of $z/D = 41.5$, 82.8 and 113 respectively and their measurements were made at 11 radial locations of $r/R = 0$, 0.2, 0.4, 0.5, 0.6, 0.7, 0.75, 0.8, 0.85, 0.9, 0.95 to get the local flow parameters of the adiabatic air–water two-phase flow.

The conical multi-sensor probe was manufactured by pull-cutting a optical fiber locally heated by a thin flame from a gas burner. The details of the probe methodology can be found in the literatures [8–10]. The WE7000 control data acquisition system from the Yokogawa electric corporation is used with optical probes.

In order to verify the accuracy of local probe measurements, the area-averaged void fraction obtained by integrating the locally measured time-averaged void frac-

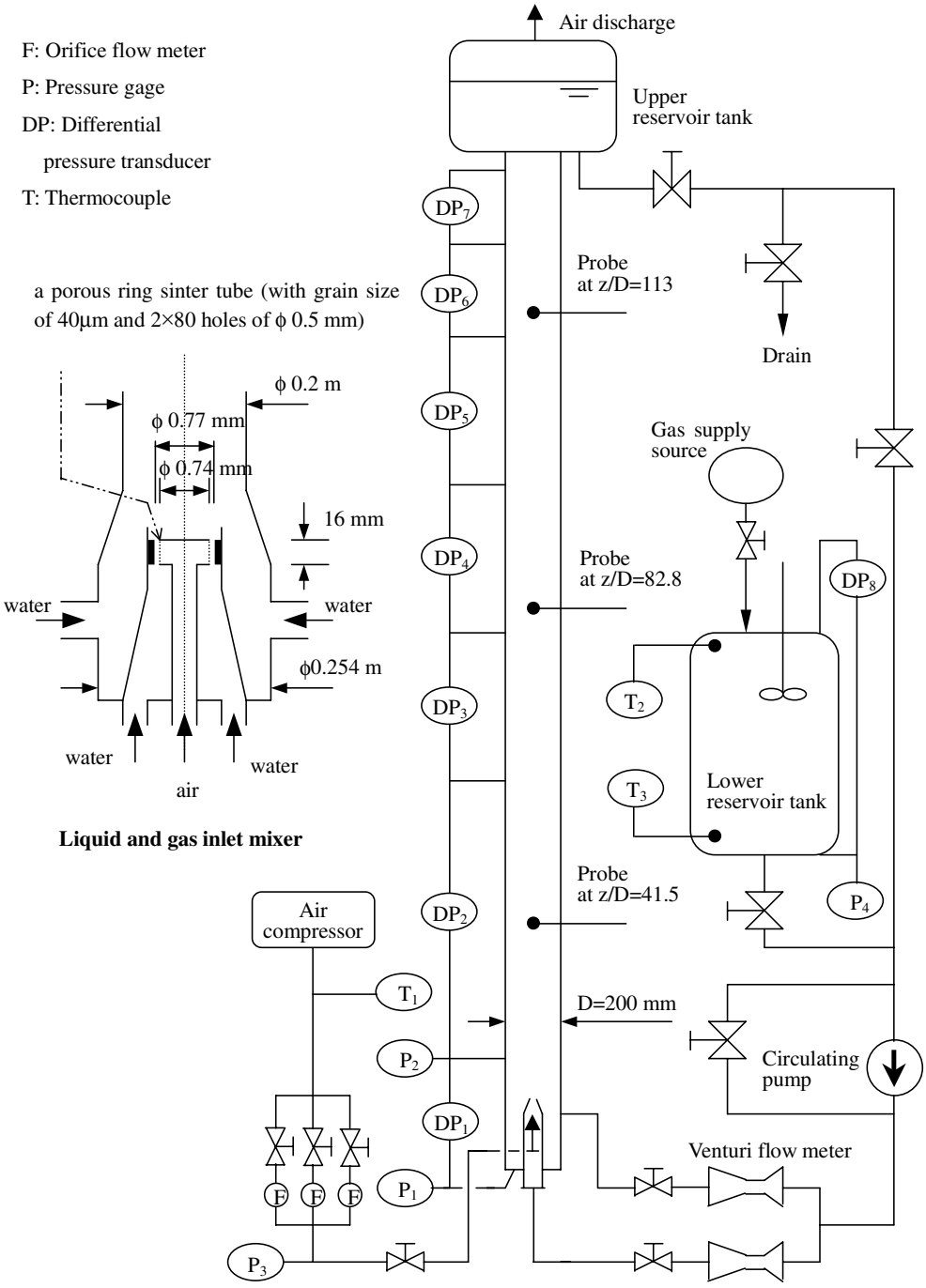

Fig. 1. Schematic diagram of test loop at Large Scale Test Facility (LSTF).

tion over the flow channel was compared with that measured by the differential pressure transducers. The comparison showed that reasonably good agreements were reached and the average ratio of the probe measurement to the pressure transducer measurement was 0.9815.

2.3. Experimental ranges

The adiabatic air–water flow experiments were performed under the flow conditions ranged from 0.0311 to 0.372 m/s for the area-averaged superficial gas velocity,

j_g and from 0.0350 to 0.277 m/s for the area-averaged superficial liquid velocity, j_f The area-averaged superficial gas and water velocities, j_g and j_f are estimated using the static pressure at the top of the test section.

3. Results and discussion

3.1. Phase distribution pattern

Figs. 2–5 show the behavior of void fraction profiles measured at $z/D = 41.5$ (bottom), 82.8 (middle) and 113 (top) for $j_g = 0.0311$, 0.0810, 0.186 and 0.372 m/s respectively. The phase distribution is linked with local parameters that govern the local flow conditions, such as phase velocities, size distribution and configuration of bubbles or interfaces. The bubble size distribution and configuration reflect specifically on the nature of both bubble behaviors and two-phase flow turbulence and are determined by the bubbly drag force that is governed by the distortion and swerving motion of the bubble.

In two-phase systems with heat addition, Ishii [1] divided the radial void fraction profiles into concave and convex profiles and pointed out that the profile changes from concave to convex in the heating vertical flow direction. Based on the experiments performed by different researchers with different types of bubble injections in round tubes ($20 \leqslant D \leqslant 86.4$ mm), Serizawa and Kataoka [2] classified the phase distribution patterns into four basic types of the distributions, that is, wall peak, intermediate peak, core peak, and transition. The wall peak distribution is characterized by a sharp peak with relatively high void fraction near the channel wall and plateau with very low void fraction around the channel center. The intermediate peak is explained as broad peak in void fraction near the channel wall and plateau with medium void fraction around the channel center. The core peak is defined as broad peak around the channel center and no peak near the channel wall. The transition is described as two broad peaks around the channel wall and center. Hibiki et al. [3] studied the phase distribution pattern in an annulus with hydraulic equivalent diameter of 19.1 mm in their own way and divided the bubbly flow region into four regions: (1) bubble-mixing region where the bubble-induced turbulence is dominant (at low void fraction and low liquid velocity ($\alpha \leqslant 0.25$, $j_f \leqslant 0.3$ m/s)), (2) region where the wall peak appears (at low void fraction and medium liquid velocity ($\alpha \leqslant 0.25$, $0.3\text{ m/s} \leqslant j_f \leqslant 5\text{ m/s}$)), (3) region where the core peak appears (high void fraction ($\alpha \geqslant 0.25$)), and (4) bubble-mixing region where the shear-induced turbu-

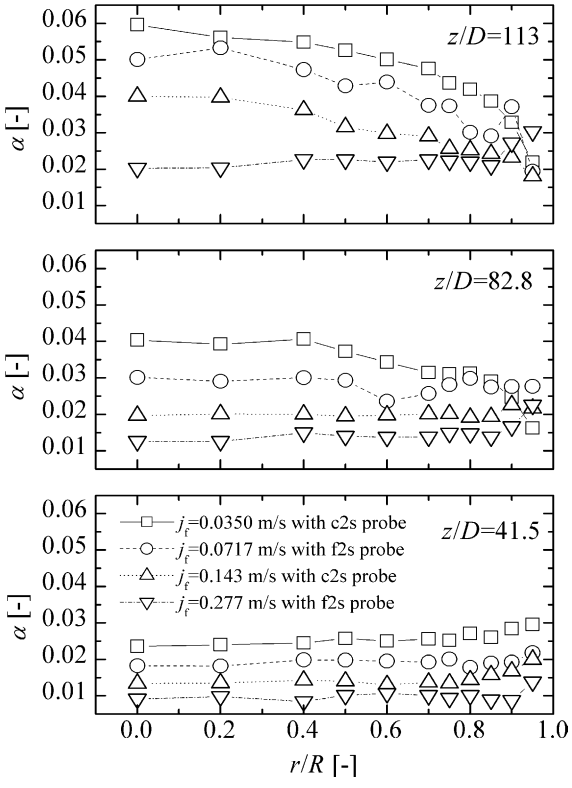

Fig. 2. Void fraction profile of $j_g = 0.0311$ m/s.

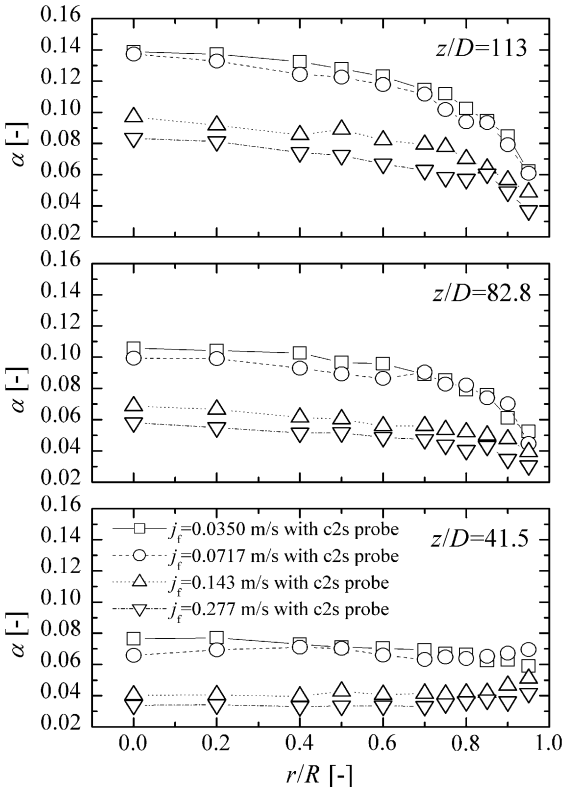

Fig. 3. Void fraction profile of $j_g = 0.0810$ m/s.

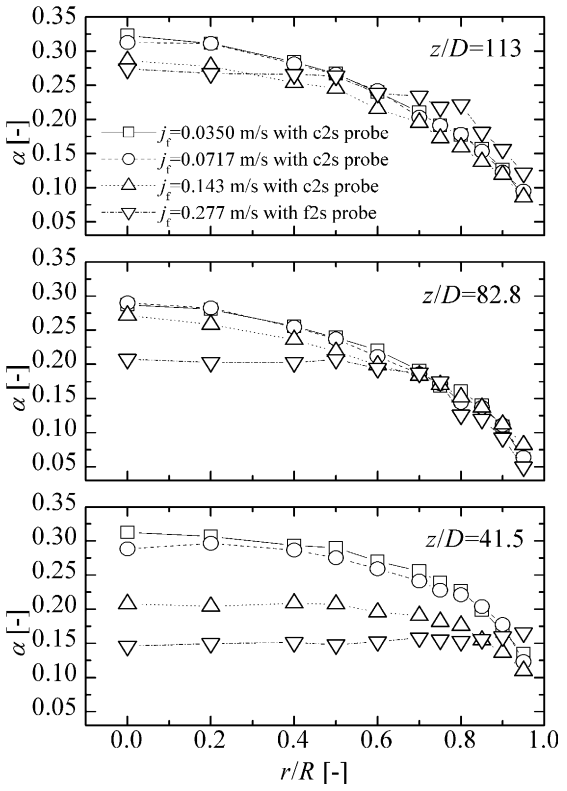

Fig. 4. Void fraction profile of $j_g = 0.186$ m/s.

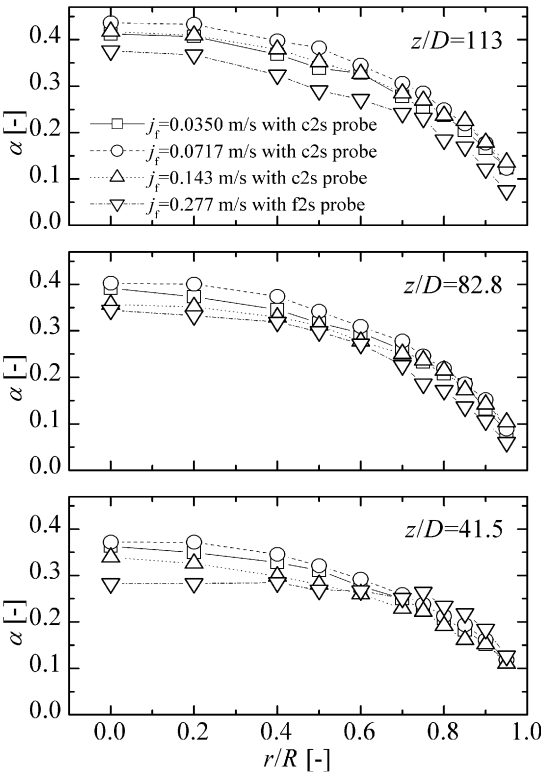

Fig. 5. Void fraction profile of $j_g = 0.372$ m/s.

lence is dominant (low void fraction and high liquid velocity ($\alpha \leqslant 0.25$, $j_f \geqslant 5$ m/s)). They also pointed out that the intermediate peak and transition categorized by Serizawa and Kataoka [2] may be the transition between regions (4) and (2) or (3), and the transition between regions (1) and (2) or (3), respectively. Ohnuki and Akimoto [4] investigated the phase distribution in the upward air–water two-phase flow along a large diameter pipe with 200 mm in inner diameter (D) and 61.5 in height-to-diameter ratio (z/D) and classified the phase distribution near the top of the vertical large diameter pipe into wall peak and core peak phase distribution patterns only. The present experimental study in the vertical large diameter pipe with 200 mm in inner diameter and 120 in height-to-diameter ratio shows that no intermediate peak phase distribution pattern suggested by the Serizawa–Kataoka's map [2] was found in the large diameter pipe and the characteristic of the transition phase distribution pattern suggested by the Serizawa–Kataoka's map [2] was also not pronounced. As a result of that, the phase distribution patterns in the large diameter pipe could be classified into two basic types of the phase distributions, namely, wall peak and core peak.

In order to quantitatively analyze phase distribution patterns in the two-phase flow, we introduced the concept of the skewness, which stands for the degree of asymmetry of a distribution. If the distribution has a longer tail less than the maximum, the function has negative skewness. Otherwise, it has positive skewness. Several types of skewness are defined. The Fisher skewness (the most common type of skewness, usually referred to simply as the "skewness") is defined by

$$\gamma = \frac{B_3}{B_2^{1.5}}, \tag{1}$$

where B_i is the ith central moment.

For the flow in the channel, the first raw moment or the expectation value, namely a simple area average over the cross-sectional area A, can be given by

$$\langle F \rangle = \frac{1}{A}\int_A F \,\mathrm{d}A. \tag{2}$$

And the second and third central moment can be given respectively by

$$B_2 = \langle (F - \langle F \rangle)^2 \rangle = \frac{1}{A}\int_A (F - \langle F \rangle)^2 \,\mathrm{d}A, \tag{3}$$

$$B_3 = \langle (F - \langle F \rangle)^3 \rangle = \frac{1}{A}\int_A (F - \langle F \rangle)^3 \,\mathrm{d}A. \tag{4}$$

In the analysis of the phase distribution in a cross-sectional area of the vertical large diameter pipe, we would set $F = \alpha(r)$ and can obtain the expectation

value of void fraction, the second and third central moment, respectively, over the cross-sectional area $A = \pi R^2$,

$$\langle \alpha \rangle = \int_0^R \frac{\alpha(r) \cdot 2r}{R^2} \, \mathrm{d}r, \tag{5}$$

$$B_2 = \int_0^R \frac{(\alpha(r) - \langle \alpha \rangle)^2 \cdot 2r}{R^2} \, \mathrm{d}r, \tag{6}$$

$$B_3 = \int_0^R \frac{(\alpha(r) - \langle \alpha \rangle)^3 \cdot 2r}{R^2} \, \mathrm{d}r. \tag{7}$$

When the skewness, γ, has a negative value, it indicates a core peak phase distribution pattern in the two-phase flow. Otherwise, it has a wall peak phase distribution pattern. The larger $|\gamma|$ is, the broader or sharper the core or wall peak is. $|\gamma| = 0$ shows the change between the wall peak and core peak phase distribution, corresponding to the radial even phase distribution. The analysis showed that the skewness can distinguish the phase distribution pattern quantitatively, instead of the shape observation in the conventional qualitative judgment, could deal with the continuity of phase distribution transition and involved it in the present two-phase flow theory in mathematical language.

In Fig. 6, the Fisher skewnesses at $z/D = 41.5$ and 82.8 and 113 respectively are plotted against the superficial gas velocity as a parameter of the superficial liquid velocity. It is noted that $|\gamma| \leqslant 2$ in the experimental range, which reveals that a nearly flat radial void fraction profile with relatively steep decrease (corresponding to core peak phase distribution) or increase (corresponding to wall peak phase distribution) in the void fraction near the wall prevails in the upward adiabatic air–water two-phase flow in the vertical large diameter pipe. This may be attributed to strong mixing due to bubble-induced turbulence or secondary flow, since it would dominate the flow in the large diameter pipe, especially in low liquid velocity and high gas velocity flow conditions. Approximate trends of the core and wall peak depending on the superficial gas velocity, the superficial liquid velocity and the z/D can be observed in Fig. 6. As the superficial liquid velocity increases, the skewness increases too and the corresponding phase distribution becomes less core peaking or more wall peaking, or changes from core peaking to wall peaking. If the superficial liquid velocity equals to zero (two-phase pool experiment), the skewness would have a large negative value and the corresponding phase distribution would have a broad core peak. The positive skewness increase indicates that the wall peak becomes sharper and moves towards the channel wall, and the absolute value of the negative skewness increase shows that the core peaking becomes larger and the void fraction at the peak is being augmented. As general trends in Fig. 6, the increase in the superficial gas velocity decreases the skewness and

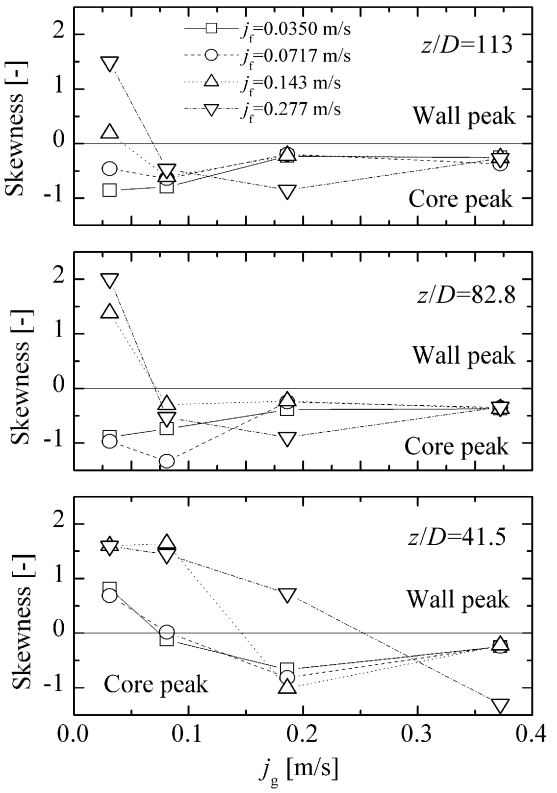

Fig. 6. Skewness for phase distribution.

the corresponding phase distribution becomes more core peaking or less wall peaking, or changes from wall peaking to core peaking. As z/D increases and the air–water two-phase flow develops along the vertical large pipe, the skewness also decreases and the corresponding phase distribution also becomes more core peaking or less wall peaking, or changes from wall peaking to core peaking.

It is known that the wall peaking phase distribution flow pattern might be formed due to the transversal lift force acting on bubbles moving in a shear flow with radial velocity gradient at relatively low superficial gas velocity under which condition bubbles are rather small and spherical or near spherical in their shape. On the other hand, the core peaking phase distribution flow pattern might be formed by larger and deformed bubbles. The radial velocity gradient is the dominant factor in the determination of the transversal motion of bubbles and the bubble coalescence and breakup play an important role in the determination of the bubble size.

3.2. Phase distribution pattern transitions

Since no quantitative relationships were given by Ishii [1], Serizawa and Kataoka [2], Hibiki et al. [3] and Ohnuki and Akimoto [4,5] to distinguish the wall and intermediate peaks, the classification between the

core and wall peaks in the present study were performed by using the current phase distribution change criterion from core to wall peak, $|\gamma| = 0$. First, we assumed that the phase distribution change depends on gas Reynolds number, $Re_g = \frac{\rho_g j_g D}{\mu_g}$, where ρ_g, μ_g and j_g are the gas density, the gas viscosity and superficial gas velocity respectively, and on liquid Reynolds number, $Re_f = \frac{\rho_f j_f D}{\mu_f}$, where ρ_f, μ_f and j_f are the liquid density, the liquid viscosity and superficial liquid velocity respectively. Then, by the application of the criterion and the data of the present study, the criterion for the phase distribution change from wall to core peak, $|\gamma| = 0$, can be fitted by the following empirical relation:

$$\frac{z}{D} = 128 Re_g^{-0.7} Re_f^{0.39}, \tag{8}$$

where z/D is the height to inner diameter ratio of the large diameter pipe, and j_g, j_f and gas and liquid properties are estimated by using the pressure and temperature of the system.

Eq. (8) indicates that the phase distribution pattern changes along the flow direction from wall peaking to core peaking increases in the flow direction with the increasing superficial liquid velocity and the decreasing superficial gas velocity. When the superficial liquid velocity equals to zero in the two-phase in a pool or the superficial gas velocity approaches to infinite, the phase distribution pattern transition from wall peak to core peak happens at $z/D = 0$, that is to say, only core peak phase distribution pattern exists in two-phase flow with a very small superficial liquid velocity or a very large superficial gas velocity. When the superficial liquid velocity approaches to infinite or the superficial gas velocity equals to zero, the phase distribution pattern transition from wall peak to core peak happens at $z/D = \infty$, that is to say, only wall peak phase distribution pattern exists in two-phase flow with a very large superficial liquid velocity or a very small superficial gas velocity.

In Fig. 7, we compared Eq. (8) and Serizawa–Kataoka's map [2] with the phase distribution patterns observed at $z/D = 41.5$, 82.8 and 113 in this experiment, based on which the Eq. (8) was fitted. In order to validate Eq. (8), it was also compared with the phase distribution patterns measured at $z/D = 33$, 43 and 60 in the large diameter pipe experiment of Sun et al. [11] (101.6 mm in inner diameter), Shoukri et al. [12] (200 mm in inner diameter) and Ohnuki and Akimoto [4] (200 mm in inner diameter) in Fig. 8. The symbols of triangle and square in Figs. 7 and 8 denote the core and wall peak phase distribution patterns respectively. The solid and broken lines in Figs. 7 and 8 are, respectively, the phase distribution transition boundaries predicted by Eq. (8) and the phase distribution pattern transition boundaries developed by Serizawa and Kataoka [2]. Figs. 7 and 8 reveal that the phase distribution patterns observed at various z/D in the vertical large

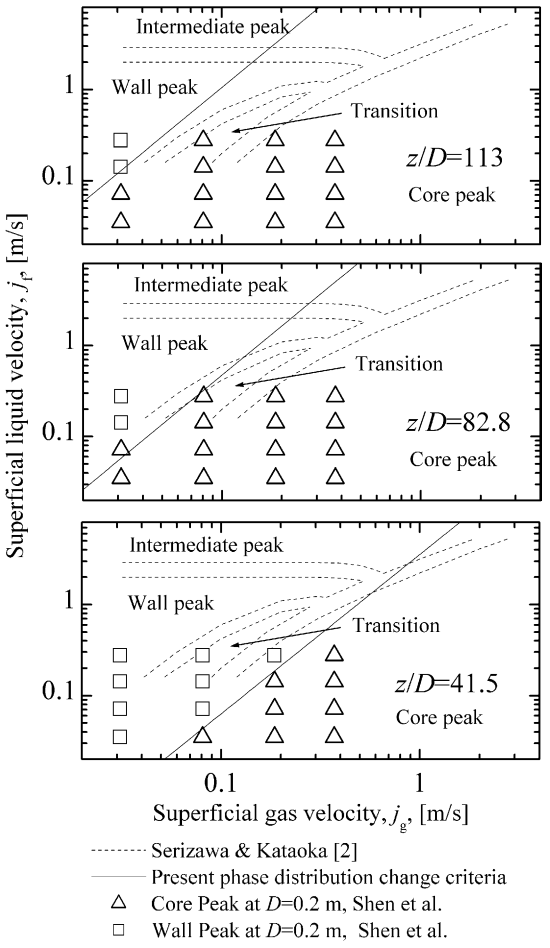

Fig. 7. Map of phase distribution patterns and comparison with the present data.

diameter pipe by different researchers do not agree well with the Serizawa–Kataoka's map [2] at most of the flow conditions. However, Eq. (8) can predict the wall and core peak phase distribution pattern transitions in the large diameter pipe satisfactorily.

It should be noted that the phase distribution transition criterion, Eq. (8), has been examined against the experimental data for the flow regime in the region $z/D > 15$ but it was not examined against the inlet flow regime in the region $z/D < 15$, because the phase distribution pattern and bubble behaviors in this regime are dependent on the gas injection methods. Sekoguchi et al. [14] observed the behaviors of isolated bubbles, which were introduced into vertical water flow in a $25 \times 50\,mm^2$ rectangular channel through a single nozzle with different gas injection methods. The first method is a direct injection, in which the bubbles were injected directly to the water through a nozzle, which was inserted into the flow. This method produced distorted ellipsoidal bubbles with the length along the major axis, d_{bl}

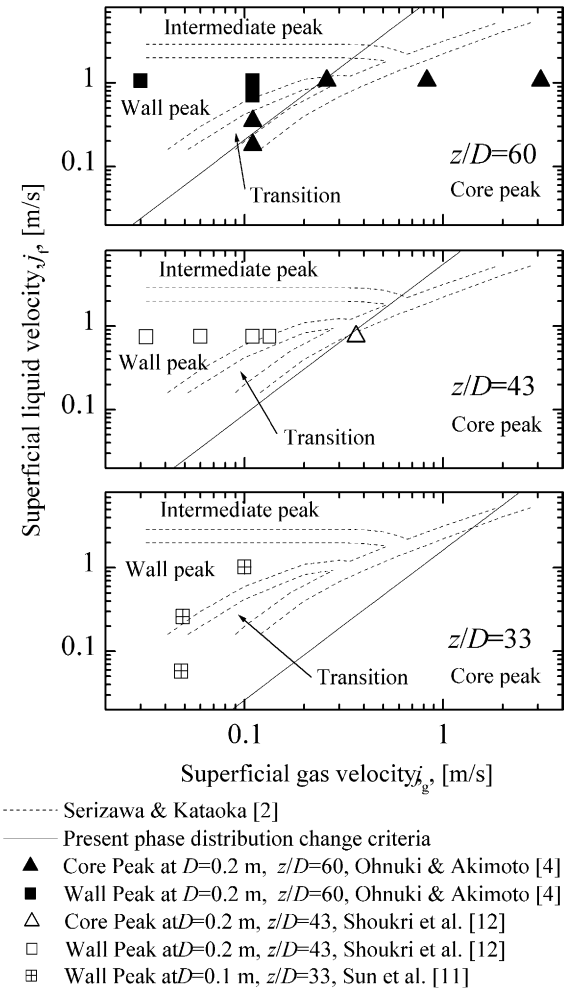

Fig. 8. Map of phase distribution patterns and comparison with other researchers' data.

ranging from 2 to 7 mm. The secondary method is an indirect injection, in which the bubbles generated in a bubble generator under the test section were entrained by water flow through a small tube and came out into the test section. This method produced almost spherical bubbles ranging from 1.8 to 3.6 mm in diameter. Based on their photographic observations, they found that the distorted ellipsoidal bubbles with a d_{bl} smaller than nearly 5 mm tended to migrate toward the wall, whereas the distorted ellipsoidal bubbles with d_{bl} larger than 5 mm rose in the channel center with oscillatory motions of the interfaces, when the direct injection was used, and that the only spherical bubbles rose in the core without oscillatory motions of the interfaces when the indirect injection was used. Hibiki et al. [3] also reported that significant interfacial area transport occurred near a test section inlet ($z/D < 15$) and gradual interfacial area transport occurred in the test section of $15 < z/D < 60$ in round tube and annulus. In consequence, although strong liquid recirculation and significant interfacial area transport occur in the inlet flow stage, it is not the typical air–water two-phase flow in the large diameter pipe. Gradual interfacial area transport occurs and inlet influence on the flow disappears in the stage of $z/D > 15$ and it can be thought that the flow in $z/D > 15$ reaches to a quasi-fully-developed flow or fully developed in the large diameter pipe and the two-phase flow characteristics of the large diameter pipe are represented by the flow in this stage.

Thus, the phase distribution transition criterion, Eq. (8), was valid for the region with $z/D > 15$ in the large diameter pipe and it need further examination in the region with $z/D < 15$ due to the inlet influence. It was also shown that Eq. (8) gave reasonably good prediction for the experimental data taken under various conditions such as flow channel diameters (0.1–0.2 m), pressure (0.1 MPa), j_f (0.0350–1.06 m/s), j_g (0.0311–3.10 m/s) and fluid system (air–water).

3.3. Time-averaged local void fraction

As described previously, the radial void fraction profiles in Figs. 2–5 do not show sharp core or wall peaking in the upward adiabatic air–water two-phase flow in the vertical diameter pipe. The nearly uniform phase distribution in the pipe core region may be attributed to strong mixing due to bubble-induced turbulence or secondary flow and the large diameter pipe provides the bubbles and bubble-induced turbulence a relatively free space to move and form. At low superficial gas velocities (j_g = 0.0311, 0.0810 and 0.186 m/s) the phase distribution pattern (at z/D = 41.5, 82.8 and 113) change from wall peaking to core peaking in the vertical flow direction. However, at a high superficial gas velocity (j_g = 0.372 m/s) the phase distribution patterns (at z/D = 41.5, 82.8 and 113) show very similar core peak phase distributions. From the tendency we can predict that the phase distribution pattern change from wall peaking to core peaking happens within the region of $z/D < 41.5$ at the high superficial gas velocity (j_g = 0.372 m/s). As the superficial liquid velocity increases, the phase distribution pattern becomes flatter core peaking and more wall peaking, or changes from core peaking to wall peaking. As the superficial gas velocity increases, the phase distribution pattern becomes more core peaking or flatter wall peaking, or changes from wall peaking to core peaking. The pheno- mena are in accordance with the previous skewness predictions.

3.4. Area-averaged void fraction

The cross-sectional area-averaged void fraction, $\langle\alpha\rangle$, is the first raw moment, namely, expectation value, of time-averaged local void fractions. Fig. 9 shows the

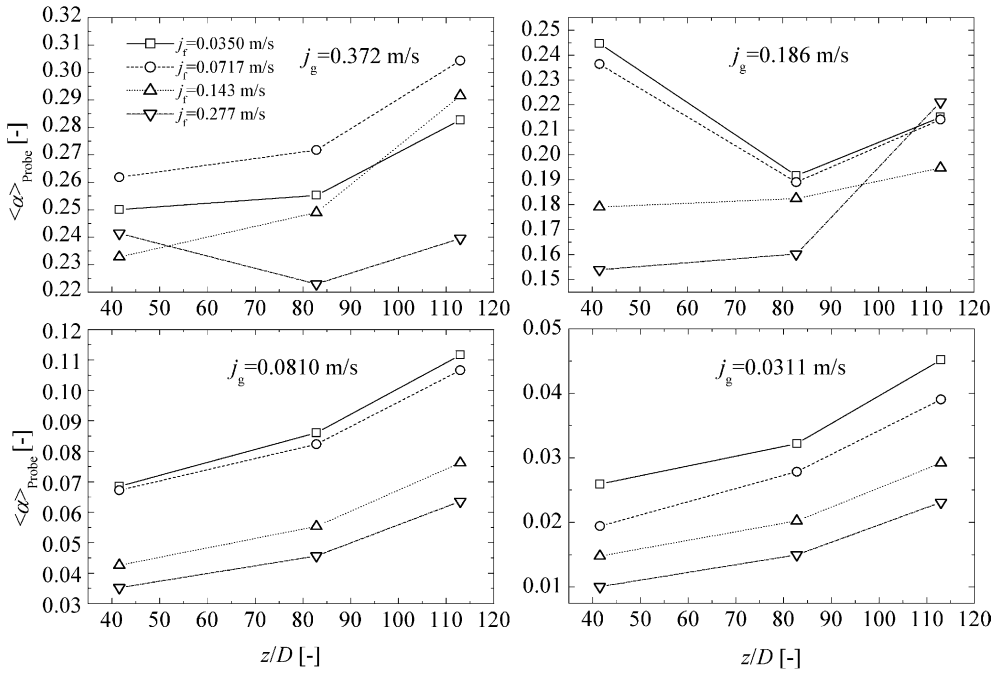

Fig. 9. Area-averaged void fractions with optical probes.

area-averaged void fractions from the optical probe measurement along the flow direction as a parameter of the superficial liquid velocity, j_f for $j_g = 0.0311$ (in right lower part), 0.0810 (in left lower part), 0.186 (in right upper part) and 0.372 m/s (in left upper part). The cross-sectional area-averaged void fraction $\langle\alpha\rangle$ increases along the flow direction at low superficial gas velocity flow condition ($j_g = 0.0311$ and 0.0810 m/s). In general, this tendency should be kept in the range of high superficial gas velocity in the vertical large diameter pipe, but in some flow condition, the cross-sectional area-averaged void fractions at low z/D show larger values than the following void fractions in the flow direction do and their corresponding local pressure losses significantly decrease (see Fig. 14) due to the flow plugging phenomena, which will further be discussed in Section 3.6. The cross-sectional area-averaged void fraction increases with the superficial gas velocity. When the superficial liquid velocity increases, the cross-sectional area-averaged void fraction decreases generally, but in some conditions of low superficial liquid velocity and high superficial gas velocity, the area-averaged void fraction locally increases with the superficial liquid velocity increase due to the flow plugging phenomena (see the downward triangle at $z/D = 41.5$ when $j_g = 0.277$ m/s in Fig. 9). These characteristics of cross-sectional area-averaged void fractions can also be seen in Fig. 10, which shows the cross-sectional area-averaged void fraction with differential pressure transducers (refer to Section 4) along the flow direction as a parameter of the superficial liquid velocity, j_f for $j_g = 0.0311$ (bottom right), 0.0810 (bottom left), 0.186 (top right), 0.372 m/s (top left).

The wall peak phase distribution patterns occur in the low area-averaged void fraction ranges. In the range of $\langle\alpha\rangle < 0.03$, the present result shows that only wall peak phase distribution patterns appear in vertical large diameter pipe. In the range of $0.03 < \langle\alpha\rangle < 0.16$, the wall peak phase distribution pattern prevails in low z/D region. The core peak phase distribution patterns develop from the wall peak phase distribution patterns as the two-phase flow develops in confined flow space, because the lighter phase tends to migrate into the higher velocity region [13]. The core peak phase distribution pattern prevails in the upward two-phase flow in the vertical large diameter when $\langle\alpha\rangle > 0.16$.

3.5. Bubble size

The extensive study of Ishii [1] revealed that the bubbly flow is characterized by the distortion of bubble shape and irregular motions and the bubble drag coefficient does not depend on the viscosity, but should be proportional to the bubble diameter. Sekoguchi et al. [14] also found that the bubble behaviors in dilute suspension flow might depend on the bubble size (larger than 5 mm in d_{bl} or not) for direct gas injection and bubble shape based on their experimental observations.

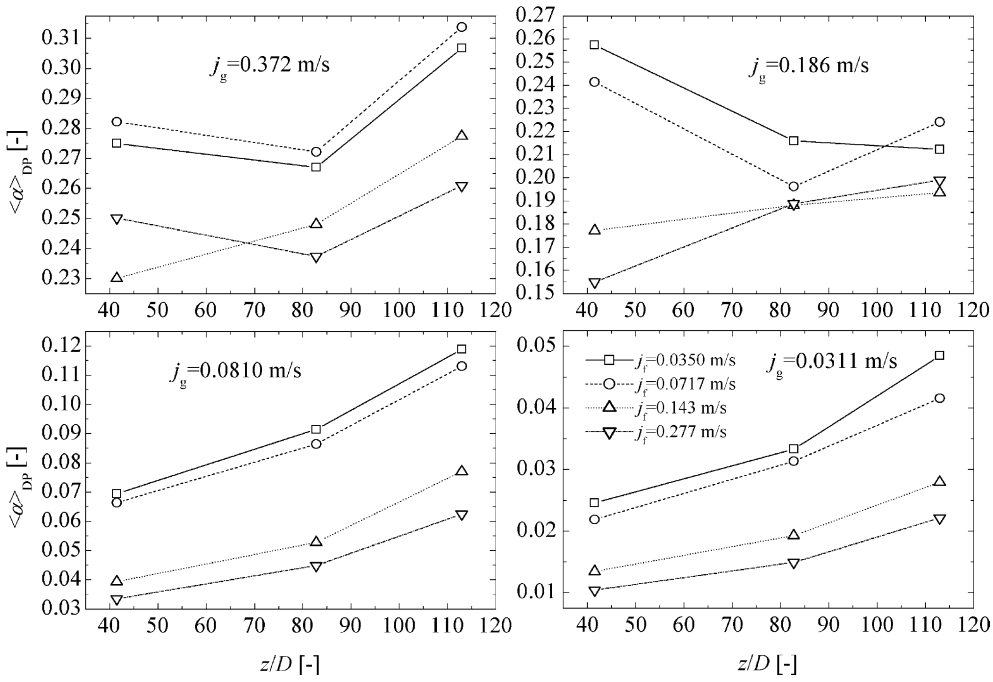

Fig. 10. Area-averaged void fractions with differential pressure transducers.

Grossetete [15] and Zun [7] also indicated that the phase distribution profile transition in air air–water bubbly flows occurs when bubbles are larger than about 5 mm in diameter. Tomiyama et al. [6] estimated the critical bubble diameter causing the radial void fraction transition from wall peaking to core peaking in an air–water bubbly flow at about 5.8 mm by evaluating the bubble net transverse lift coefficient. Hibiki and Ishii [16] measured the Sauter mean diameter in a round tube with 25.4 mm in inner diameter by a double-sensor probe and pointed out that the core peak void fraction profiles occur when the Sauter mean diameter is larger than 3.5 mm.

The Sauter mean diameter was calculated by multiplying 6 to the ratio of the time-averaged void fraction to the time-averaged interfacial area concentration. The left and right figures in Fig. 11 show the behavior of radial profiles of the Sauter mean diameter for $j_g = 0.186$ and 0.372 m/s, respectively, as parameters of j_f and z/D in the present study. The Sauter mean diameter profiles in the vertical large diameter pipe are almost uniform along the pipe radius with some decreases in size near the wall, $r/R > 0.8$. The Sauter mean diameter do not increase remarkably in the flow direction regardless of a significant pressure effect, because of the existence of dominant large bubbles (see Figs. 12 and 13). The secondary flows induced by large bubbles not only provide a chance to force the bubbles to migrate into the pipe center region, but also cause the bubbles to coalesce to form larger bubbles or to break up into smaller bubbles around the large bubbles, resulting in apparent decrease in the Sauter mean diameter with the flow development.

It appears to be difficult to distinguish the wall and core peak phase distributions in the large diameter pipe based only on the magnitude and the distribution of Sauter mean diameter. However, Ohnuki and Akimoto [4] indicated that the formation of large bubbles affects the phase distribution in a large diameter pipe. Bubble chord length distributions at $r/R = 0$ (i.e. at the center of the pipe) for $j_g = 0.186$ and 0.372 m/s were accordingly investigated to know the large bubbles in Figs. 12 and 13 by comparing with their corresponding phase distributions. The results showed that there exist very large slug bubbles with a size over the pipe diameter and the core peak phase distributions appear when the large bubbles with about 50 mm in size are formed. Before the formation of the large bubbles, both wall and core peak phase distribution could be developed and it is difficult to determine the condition for phase distribution transition in this region by using the bubble size only as done by some of the above-mentioned researchers.

3.6. Differential pressure

Fig. 14 compared the axial distribution of sectional differential pressure under various flow rates. The differential pressure decreases with the increasing superficial

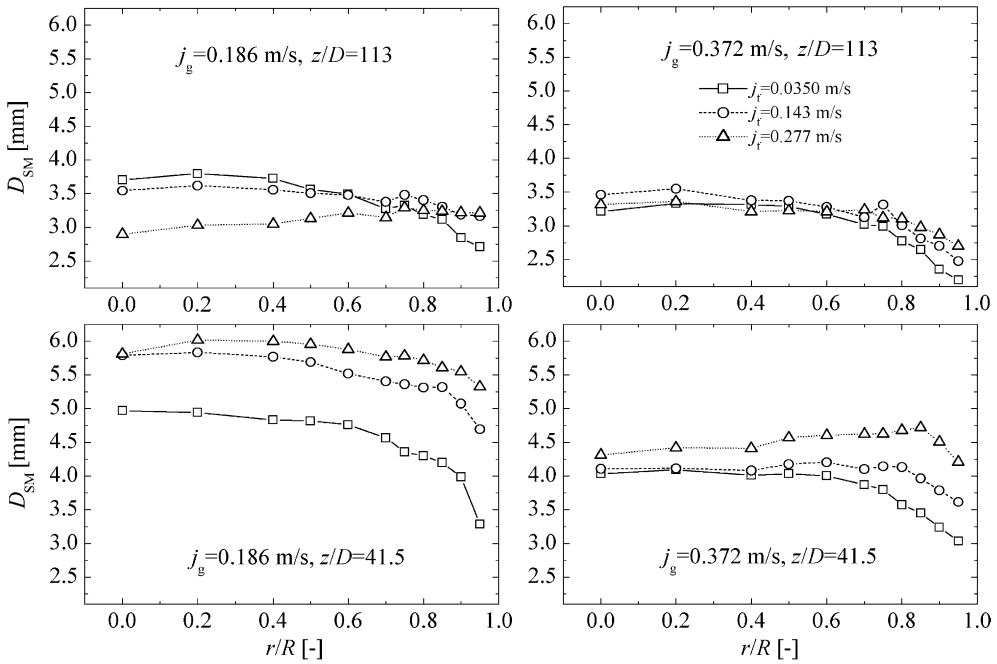

Fig. 11. Radial profile of Sauter mean diameter of j_g = 0.186 and 0.372 m/s.

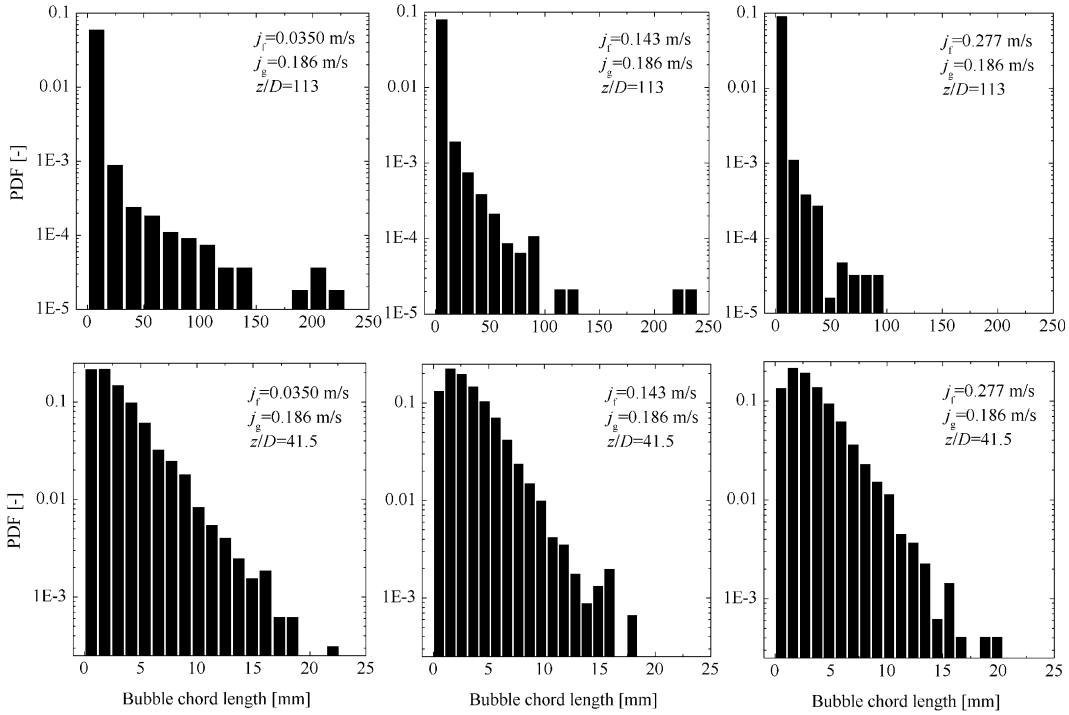

Fig. 12. PDF of bubble chord length at r/R = 0 for j_g = 0.186 m/s.

gas velocity due to the fact that the void fraction increases with superficial gas velocity and the increase of frictional pressure loss is not significant. In most cases, the differential pressure increases with the increasing

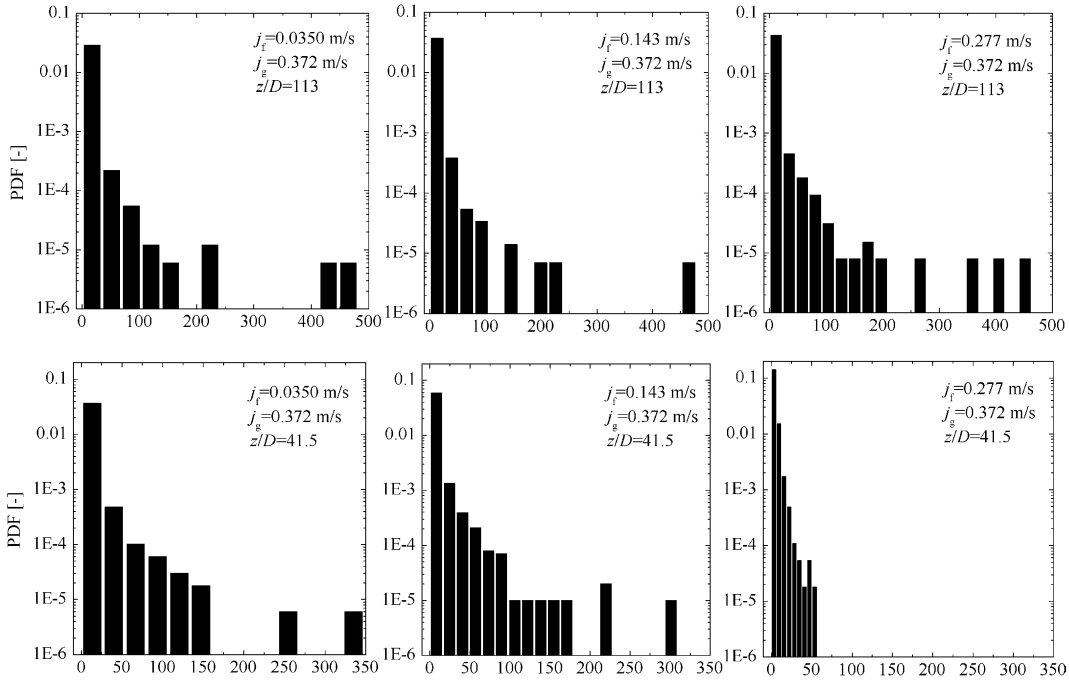

Fig. 13. PDF of bubble chord length at $r/R = 0$ for $j_g = 0.372$ m/s.

superficial liquid velocity and decreases along the flow direction. This is not the case, however, at a high superficial gas velocity and a low superficial liquid velocity condition, and the local pressure loss in the range of $z/D = 10$–60 in particular is low due to the plugging phenomena. The phenomena can also be observed in the axial profile of the cross-sectional area-averaged void fraction in Figs. 9 and 10, where the cross-sectional area-averaged void fractions show particularly high values at $z/D = 41.5$ at high superficial gas and low superficial liquid velocities. The plugging phenomena are corresponding to the churn or slug flow regime and the core peak phase distribution pattern. The plugging position moves toward lower z/D region as the superficial gas velocity increases. The void fraction may play an important role in the formulation of the plugging phenomena. When the gas flow rate from the nozzle is sufficiently high, the gas phase accumulates downstream of the gas injection nozzle due to the large drag force and limited relative velocity between two phases, and when the void fraction exceeds 0.2, the probability of bubble collision and consequent coalescence becomes very large to form a large coalesced bubble in the flow-developing region, which can be seen from the bubble chord length distribution at $z/D = 41.5$ in Figs. 12 and 13. As a result of that, the significant decrease in the axial local pressure loss and the significant increase in the axial local void fraction appear in the flow.

In the wall peak phase distribution pattern, almost linear relationship between the differential pressure and height-to-diameter ratio is attained. It may be ascribable to the low void fraction and the low bubble collision frequency, and consequently the pressure change along the flow mainly depends on the static pressure change. Comparing with the wall peak phase distribution pattern, the core peak phase distribution pattern is more complicated. In the core peak phase distribution and undisturbed bubbly flow regime, a linear relationship between the differential pressure and height-to-diameter ratio can be kept, while in the core peak phase distribution and agitated flow regimes, a good linear relationship can not be kept due to the surge of the large bubbles or bubble clusters.

4. Verification of the measurement

This study measured the cross-sectional area-averaged void fractions with both probes and differential pressure transducers to ensure the reliability of the measurement. The measured results are shown in Figs. 9 and 10 respectively. The void fraction measured by a differential pressure transducer was the volume-averaged void fraction, which was assumed to be represented by a cross-sectional area-averaged void fraction at the axial center of the measuring volume. The required cross-sectional area-averaged void fraction at a certain axial posi-

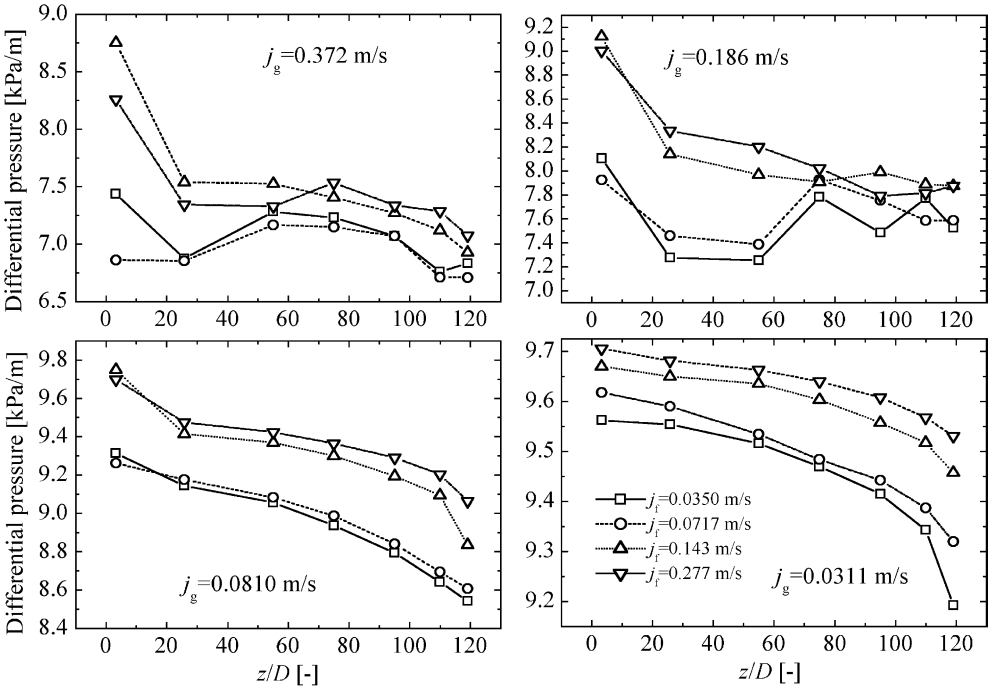

Fig. 14. Axial distribution of sectional differential pressure.

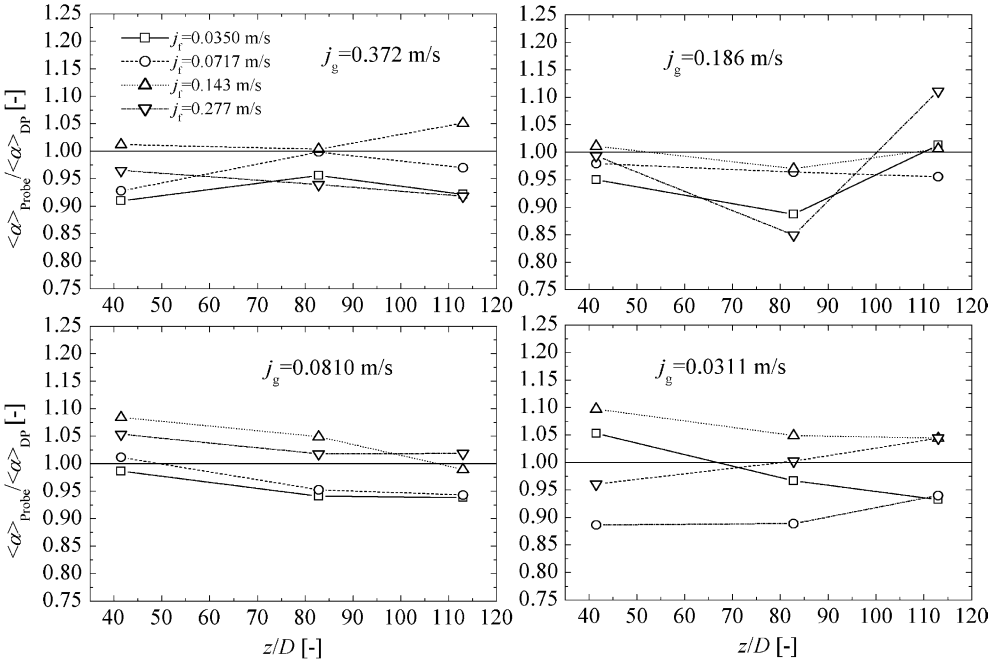

Fig. 15. Ratios of area-averaged void fraction with probes and differential pressure transducers.

tion was calculated from the cross-sectional area-averaged void fractions at the axial center of the two adjacent measuring volumes with differential pressure transducers by interpolation. Fig. 15 displays the ratios

Table 1
Wall and core peak phase distribution pattern characteristics in a vertical large diameter pipe

Phase distribution patterns	Wall peak	Core peak
Causes of formation	(1) Net liquid velocity (2) Low j_g (3) Radial velocity gradient	(1) Bubble coalescence and breakup (2) Radial velocity gradient
Peak shape	Almost uniform along the radius with some increase near wall	Nearly uniform along the radius in the core and some decreasing near wall
Skewness	>0	<0
Void fraction	Low ($\langle\alpha\rangle < 0.16$)	High ($\langle\alpha\rangle > 0.16$)
Pressure loss	Linear dependence on the z/D	(1) Linear dependence on the z/D in undisturbed bubbly flow regime (2) Almost no linear dependence on the z/D in agitated flow regimes
Flow plugging	No flow plugging	Flow plugging occurs when ($\langle\alpha\rangle > 0.2$)
Bubble size	(1) Core peaks occur if large bubbles with 50 mm in size are formed (2) Before the formation of the large bubbles, it is difficult to distinguish the phase distribution profile by the bubble size only.	
Phase distribution pattern transition	$\frac{z}{D} = 128Re_g^{-0.7}Re_f^{0.39}$	

of area-averaged void fraction with probe and differential pressure transducers, $\frac{\langle\alpha\rangle_{Probe}}{\langle\alpha\rangle_{DP}}$, under various flow conditions. The comparison shows that the agreement of the two methods is reasonably good and the $\frac{\langle\alpha\rangle_{Probe}}{\langle\alpha\rangle_{DP}}$ ranges from 0.85 to 1.10 and the average $\frac{\langle\alpha\rangle_{Probe}}{\langle\alpha\rangle_{DP}}$ in the present experiment is 98.15%.

5. Conclusions

The two-phase flow in a large diameter pipe is of great importance not only in the practical engineering application, but also in research field. In view of this, the characteristics and phase distribution patterns of two-phase flow in vertical large diameter pipe have been experimentally and theoretically studied for various flow conditions. The local measurements of the interfacial parameters (void fraction, Sauter mean diameter and pressure loss) in a vertical upward air–water two-phase flow in a 0.2 m inner diameter and 24 m in height pipe have been performed by using the optical probes and differential pressure transducers. The analysis of the experimental data showed that there exists two phase distribution patterns, namely, wall peak and core peak in upward air–water two-phase flow in the vertical large diameter pipe. The characteristics of the two phase distribution patterns are summarized in Table 1. With the application of the concept of skewness, a phase distribution pattern transition criterion was quantitatively established and the phase distribution patterns in the vertical large diameter pipe were consequently distinguished. An empirical relation for the phase distribution transition from wall peak to core peak was fitted by using the phase distribution pattern transition criterion and the present experimental data and justified by other researchers' experimental data. This study also showed that there existed the flow plugging phenomena in the low region of the test section at high superficial gas velocity conditions in the vertical large diameter pipe. The measurement with optical probe and differential pressure transducers were verified with each other finally.

Acknowledgments

This work was performed under the auspices of Japan Atomic Energy Research Institute (JAERI). The authors would like to express their sincere appreciation to the stuff of JAERI for their helps in the experiments. Part of this work was supported by Center of Excellence (COE), Japan.

References

[1] M. Ishii, One-dimensional drift-flux model and constitutive equations for relative motion between phases in various two-phase flow regimes, in: ANL-77-47, USA, 1977, pp. 1–61.

[2] A. Serizawa, I. Kataoka, Phase distribution in two-phase flow, in: N.H. Afgan (Ed.), Transient Phenomena in Multiphase Flow, Hemisphere, Washington, DC, 1988, pp. 179–224.
[3] T. Hibiki, R. Situ, Y. Mi, M. Ishii, Experimental study on interfacial area transport in vertical upward bubbly two-phase flow in an annulus, Int. J. Heat Mass Transfer 46 (3) (2003) 427–441.
[4] A. Ohnuki, H. Akimoto, Experimental study on transition of flow pattern and phase distribution in upward air–water two-phase flow along a large vertical pipe, Int. J. Multiphase Flow 26 (3) (2000) 367–386.
[5] A. Ohnuki, H. Akimoto, An experimental study on developing air–water two-phase flow along a large vertical pipe: effect of air injection method, Int. J. Multiphase Flow 22 (6) (1996) 1143–1154.
[6] A. Tomiyama, H. Tamai, I. Zun, S. Hosokawa, Transverse migration of single bubbles in simple shear flows, Chem. Eng. Sci. 57 (11) (2002) 1845–1858.
[7] I. Zun, Transition from wall void peaking to core void peaking in turbulent bubbly flow, in: N.H. Afgan (Ed.), Transient Phenomena in Multiphase Flow, Hemisphere, Washington, DC, 1988, pp. 225–233.
[8] T. Hibiki, T. Hogsett, M. Ishii, Local measurement of interfacial area, interfacial velocity and turbulence in two-phase flow, Nucl. Eng. Design 184 (2–3) (1998) 287–304.
[9] I. Kataoka, M. Ishii, A. Serizawa, Local formulation and measurements of interfacial area concentration in two-phase flow, Int. J. Multiphase Flow 12 (4) (1986) 505–529.
[10] X. Shen, Y. Saito, K. Mishima, H. Nakamura, Improved measurement method for interfacial area concentration in a large diameter tube, in: Proceeding of the 6th ASME–JSME Thermal Engineering Joint Conference, Hawaii Island, Hawaii, 2003, Paper no. TED-AJ03-389.
[11] X. Sun, T.R. Smith, S. Kim, M. Ishi, J. Uhle, Interfacial area of bubbly flow in a relatively large diameter pipe, Exp. Thermal Fluid Sci. 27 (1) (2002) 97–109.
[12] M. Shoukri, B. Stankovic, I. Hassan, J. Dimmick, Effect of pipe diameter on flow pattern transitions and void fraction of air–water flow in vertical pipes, in: Proceedings of 8th International Conference on Nuclear Engineering, Baltimore, MD, 2000, Paper No. 8285.
[13] S.G. Bankoff, A variable density single-fluid model for two-phase flow with particular reference to steam–water flow, J. Heat Transfer, Trans. ASME 82 (1960) 265–270.
[14] K. Sekoguchi, T. Sato, T. Honda, Two-phase bubbly flow (first report), Trans. JSME 40 (1974) 1395–1403 (in Japanese).
[15] C. Grossetete, Experimental investigation of void profile development in a vertical cylindrical pipe, in: A. Serizawa, T. Fukano, J. Bataille (Eds.), Advances in Multiphase Flow, Elsevier, Amsterdam, 1995, pp. 333–346.
[16] T. Hibiki, M. Ishii, Experimental study on interfacial area transport in bubbly two-phase flows, Int. J. Heat Mass Transfer 42 (16) (1999) 3019–3035.